

## **Manufacturing Letters**

Manufacturing Letters 41 (2024) 841-849



52nd SME North American Manufacturing Research Conference (NAMRC 52, 2024)

# Electric field-assisted micro-scale direct ink writing for electronic textiles

Xinnian Wang<sup>a</sup>, Yong Il Kim<sup>a</sup>, Alexander L. Yarin<sup>a,b</sup>, Yayue. Pan<sup>a\*</sup>

<sup>a</sup>Department of Mechanical and Industrial Engineering, University of Illinois at Chicago, 842 W. Taylor St., Chicago, IL 60607-7022, U.S.A. <sup>b</sup>School of Mechanical Engineering, Korea University, Seoul 136-713, Republic of Korea

\* Corresponding author. Tel.: +1-312-996-8777; E-mail address: yayuepan@uic.edu

#### **Abstract**

High-performance Kevlar fabric is widely employed in protective clothing. A recent trend involves the fusion of flexible conducting materials with protective textiles to create multifunctional E-textiles with microscale circuits. Poly(3,4-ethylenedioxythiophene): poly(styrenesulfonic acid) (PEDOT:PSS) stands out as one of the most promising conducting polymers for flexible electronic applications, owing to its remarkable electrical, chemical and mechanical properties. Until recently, the production of PEDOT:PSS material on Kevlar fabric predominantly relied on dip coating and drop coating methods, presenting significant challenges for achieving microscale customized applications. Direct ink writing (DIW) has gained popularity due to its ability to fabricate a wide range of materials with programmed patterns and three-dimensional architectures, making it increasingly attractive for electronic printing. However, the rough surface of textiles and the die-swelling phenomenon exhibited by DIW printable materials have posed challenges for microscale E-textile fabrication. In previous studies, it was discovered that an electric field could facilitate material deposition on rough surfaces. This work investigates the potential to print PEDOT:PSS-based material patterns on rough textiles with a microscale resolution. It not only validated the effectiveness of the electric-field-assisted direct ink writing when printing PEDOT:PSS-based conducting inks on Kevlar but also identifies significant factors for achieving the microscale printing resolution. Additionally, this work characterizes the resistivity of the printed micro-traces and circuits. This research opens up possibilities for further exploration in customizing microscale circuits on various textiles.

© 2024 The Authors. Published by ELSEVIER Ltd. This is an open access article under the CC BY-NC-ND license (https://creativecommons.org/licenses/by-nc-nd/4.0)

Peer-review under responsibility of the scientific committee of the NAMRI/SME.

Keywords: Kevlar, PEDOT:PSS, DIW, Electrical field, Microscale; E-textile;

#### Acronym

DIW direct ink writing

eDIW electrical field assisted direct ink writing

e-textile electronics textile

PEDOT:PSS poly(3,4-ethylenedioxythiophene): poly(styrenesulfonic acid)

**DMF** dimethylformamide THF tetrahydrofuran **DMSO** dimethyl sulfoxide polyethylene oxide PEO **ECG** electrocardiography AM additive manufacturing PETE polyethylene terephthalate **PDMS** polydimethylsiloxane

PET	polyethylene terephthalate
PTA	polyester
DI	deionized
RMSD	root-mean-square deviation

#### 1. Introduction

Electronic textiles (e-textiles), also known as smart textiles, have rapidly evolved since the 20th century, offering the ability to respond to changes in environmental conditions [1]. These textiles have led to a wide array of applications, including health monitoring, medical implants, and protective clothing [2-4]. In particular, flexible protective clothing has played an important role in the military, firefighting, and aerospace industries, preventing individuals from being exposed to hazardous environmental conditions [5-7]. Consequently, researchers have become increasingly interested in flexible, lightweight, microscale, and multifunctional e-textiles. To meet these demands, various conducting materials have been integrated into textiles, including metal wires, graphene, and conducting polymers [8-10]. Among these options, conducting polymers stand out due to their light weight, affordability, excellent adhesion to flexible polymer substrates, and compatibility with diverse manufacturing processes, making them prime candidates for e-textiles [11-12].

One prominent conducting polymer is PEDOT:PSS, singled out both the academia and industry [13]. Its exceptional chemical stability, film-forming properties, and moderate stretchability make it an ideal choice [14]. Moreover, PEDOT:PSS can be dispersed in aqueous solutions and easily applied to textiles using cost-effective methods, such as spin coating and dip coating [15-16]. However, the commonly available pristine PEDOT:PSS possesses a relatively low electrical conductivity that falls short of meeting electronic requirements [17]. To enhance the electrical conductivity, conventional methods involve the use of organic solvents such as DMF, THF, and DMSO [18-20]. These dopants, however, often require significant energy or additional steps to remove them, complicating the PEDOT:PSS fabrication process. In our previous research, we discovered that 52 wt% of PEO can boost the electrical conductivity of PEDOT:PSS without the need for extra energy to eliminate the secondary dopants [21-22]. Moreover, PEDOT:PSS-52 wt.% PEO revealed an outstanding processability.

Kevlar fabric, a high-performance polymer textile known for its light weight, flexibility, heat resistance, corrosion resistance, and abrasion resistance, is frequently used in protective clothing [23]. Nevertheless, the conventional methods of applying PEDOT:PSS to Kevlar textiles rely on traditional manufacturing processes. For example, Maithani et al. employed laser technology to introduce graphene onto Kevlar sheets, subsequently applying a drop-coating of PEDOT:PSS/DMSO solution onto the graphene sheet, successfully fabricating an ECG sensor [24]. Choi et al. utilized a dip-coating technique to apply PEDOT:PSS/DMSO solution directly onto Kevlar yarn, producing conductive threads. These threads were skillfully knitted together to create functional

electronic textiles [25]. Tao et al. employed a roll-to-roll coating process to apply PEDOT:PSS onto Kevlar threads, successfully generating functional electrodes [26]. Despite the significant progress achieved by these methods, they face challenges in fabricating microscale and complex 2D or 3D conducting structures.

AM techniques, also known as 3D printing, have played a pivotal role in recent technological advancements. AM offers the promise of fabricating intricate structures customized to specific needs, surpassing traditional manufacturing processes in design freedom and freeform fabrication. Direct ink writing (DIW), an extrusion-based AM method, stands out for its capacity to create complex designs using a variety of materials, including metals, polymers, and composites [27]. For instance, Yuk et al. successfully printed 7 wt% PEDOT:PSS onto flat PETE films and PDMS films to create circuits and electrodes [28]. Wu et al. printed PEDOT:PSS on a PET substrate to manufacture flexible micro-supercapacitors [29]. However, the rough surface of textiles and microscale resolution presents challenges for DIW processing.

In our previous study, we developed a novel eDIW process by introducing an electric field around the extrusion needle [30-31]. The results demonstrated a significant impact of the electric field on stability of the DIW process, enabling printing of low-viscosity materials not only on flat surfaces but also on rough surfaces such as PTA belts and woven cotton belts [30]. Additionally, it expanded the boundaries of printing speed limitations and improved printing resolution. Plog et al. demonstrated that low-viscosity materials could be printed at speeds of up to 13.2 m/s with the application of an electric field, with printed line widths approximately seven times smaller than the inner diameter of the needle [31]. This setup holds great promise for achieving high-resolution PEDOT:PSS fabrication on textiles.

In this study, the novel method was used for expanding the DIW technique's capabilities in fabricating high-resolution conductive lines on rough textiles, specifically Kevlar fabric. We conducted a comprehensive analysis of how various printing parameters—such as standoff distance, printing speed, and electric field strength-impact the effectiveness of Edit printing using PEDOT:PSS-PEO composite ink. In addition, we performed an in-depth analysis of the resistivity of printed lines of different widths. This article is structured as follows. Section 2 presents the materials and methods used, encompassing preparation of PEDOT:PSS-PEO ink, the eDIW setup, characterization of the printed lines, and the measurements of their electrical resistivity. Section 3 describes a comprehensive exploration of how these three selected parameters (the standoff distance, the printing speed, and the electric field strength) impact the width of the printed lines. This section also elucidates a relationship between the width of the drawn line and its resistivity. Finally, Section 4 draws comprehensive conclusions of the findings from this research.

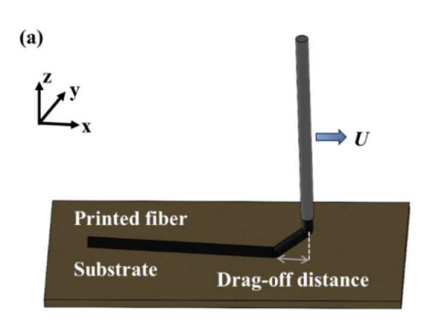
#### 2. Materials and methods

#### 2.1 Materials

PEDOT:PSS pellets, sourced from Sigma-Aldrich (USA), were initially mixed with DI water to achieve a concentration of 4.33 wt% in the resulting aqueous suspension. To ensure uniformity, the mixture was stirred at room temperature for 24 h. Subsequently, PEO was added to the 4.33 wt% PEDOT:PSS suspension. Note that the amount of PEO inserted was 52% compared to the total solute weight (i.e., the PEO weight + PEDOT:PSS weight). Then the blend was stirred for 24 h and it is denoted as PEDOT:PSS-PEO. As shown in the previous study [22], this material exhibits both shear-thinning and viscoelasticity, facilitating its printability during the process. Kevlar ballistic bulletproof fabric was used as a substrate, and it was sourced from Skarr Armor (USA).

### 2.2 Methods

The eDIW setup was developed by integrating an external electric field with a conventional DIW system (Fig. 1). The needle was grounded, and an additional governing electrode was positioned near the needle tip. The governing electrode was directly connected to a high-voltage power supply and positively charged when printing a line. During the printing process, the electric field pulled the extruded filaments from the needle toward the positive electrode, which reduced the filament drag-off distance on the substrate and hence facilitated a smooth steady-state printability of the material [30].



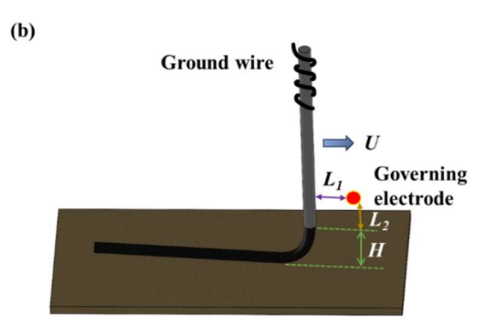


Fig.1. Schematics of the (a) DIW, and (b) eDIW process. The velocity U is the printing speed, H is the standoff distance,  $L_1$  is the horizontal distance between the electrode and the needle, and the  $L_2$  is the vertical distance between the electrode with the end of the needle.

According to Yuk et al., the diameter of the needle and the standoff distance are two dependent parameters that affect the width of printed lines [32]. Additionally, the extrusion speed and the printing speed are identified as dependent variables influencing the line width [32]. Consequently, in this study, the gauge of the needle and the air pressure were maintained as constant parameters. A 34-gauge needle (Jensen Global Inc, USA) with an inner diameter of 50 µm and a constant extrusion pressure of 76 psi was used for the eDIW presented in this paper. Three different parameters of the eDIW: the printing speed U, the stand-off distance H, and the voltage V, were varied to explore their effect. However, at very high values of H, the DIW process is significantly challenged, making the printing instable and limiting the observable effects of the electrical field. Under these conditions, only a large voltage value will be tested to evaluate the electrical field's influence at high H levels.. Each experiment was replicated five times. The printed specimens were stored at room temperature for 30 min to evaporate the entrapped water.

#### 2.3 Characterization

An optical profilometer (Bruker-Nano, Contour GT-K) was used to measure the surface morphology of the Kevlar fabric. The fabric specimens' size was  $0.61 \text{ mm} \times 0.45 \text{ mm}$ . The back scan, length, and the objective were set as 25 µm, 75 µm, and 5X, respectively. The printed line was imaged using an optical microscope (Micro-Vu, USA). Then, Python was used to find the contour to measure the width at seven different locations of the printed line for each image. Minitab software was employed to perform an analysis of variance (ANOVA), and the P-value was used to evaluate the significance of each factor (cf. the printing speed, the stand-off distance, and the electric field) on the response variable (i.e., the width of the printed line). Given the independence of the selected printing parameters, a one-way ANOVA was applied to ascertain if there were statistically significant differences among the means of these factors and to calculate the relevant statistics. In addition, a mathematical model was utilized to predict the width of the printed lines and to validate it against experimental outcomes [32]:

$$W = \frac{\alpha \times D}{\sqrt{\frac{U}{C}}} \tag{1}$$

where W represents the printed line width,  $\alpha$  is the die-swelling ratio obtained from the optical image of the free jet depicted in Fig. 2, D is the inner diameter of the needle (50µm), C is determined by the following equation:

$$C = \frac{M}{\left(\frac{\alpha \times D}{2}\right)^2 \times 3.14 \times \rho_m} \tag{2}$$

where M is the mass of the extruded filament per second  $(1.4\times10^{-3} \text{ g/s})$ ,  $\rho_{\rm m}$  is the density of the PEDOT:PSS-PEO material, which is 1.007 g/ml.



Fig. 2. Optical image of the free PEDOT:PSS-PEO jet. The  $\alpha$  is 9 times larger than the inner diameter of the needle.

To calculate the electrical resistivity  $\rho$  of the printed lines, the following equation was used:

$$\rho = \frac{R \times A}{I} \tag{3}$$

where R is the resistance of the printed line measured by a multimeter (8845A, FLUKE, USA), L is the length of the printed line, which was set as 1 mm, and A is the cross-sectional area of the printed line. The cross-section of the printed line was considered as a segment of a circle (Fig. 3), where the W and r were measured by the microscope.

$$A = \arctan\left(\frac{4rW}{W^2 - 4r^2}\right) \times \left(\frac{W^2}{8r} + \frac{r}{2}\right)^2 - \frac{W^3 - 4r^2W}{16r}$$
 (4)

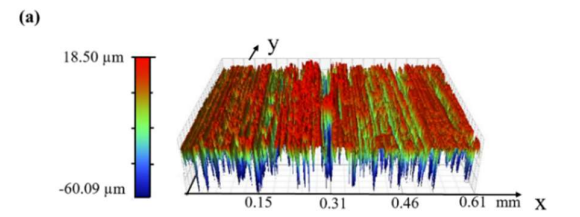


Fig. 3. Illustration of a cross-section of the printed lines drawn by the eDIW.

### 3. Results and discussion

## 3.1 Morphology of the substrate

The morphology of Kevlar fabric differed along two distinct directions. Along the y-direction, the surface was smoother, and flatter, as depicted in Fig. 4(a), with a predominant portion of the surface exhibiting a consistent height coloration, and varying by only a few microns in terms of surface roughness. However, the situation along the x-direction was markedly different. Figure 4(b) reveals a significant height variation in the -42  $\mu$ m to 19 range. This variation in the measured height, denoted as H, leads to an unstable DIW printability and hence, to printing defects or even failures on the Kevlar fabric. To validate the effectiveness of eDIW for printing patterns in arbitrary directions on the Kevlar fabric, we investigated the printing of lines in the most challenging direction, the x-direction.



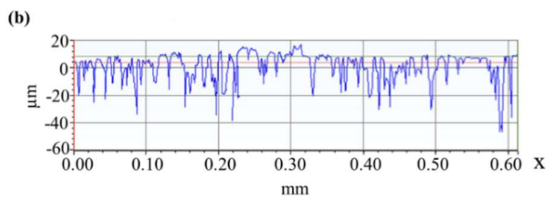
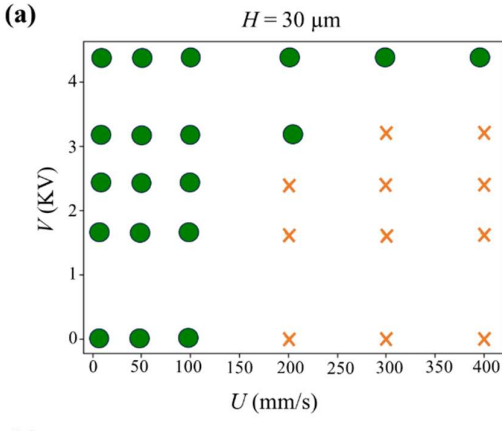


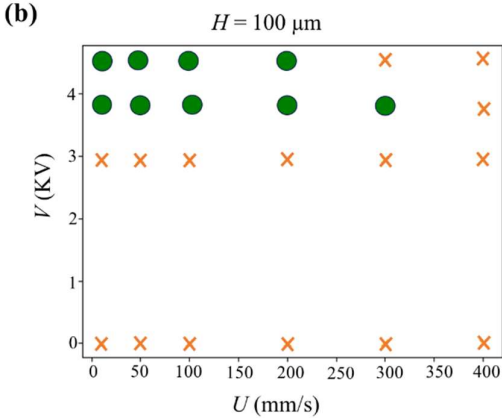
Fig. 4. Surface topographical images of Kevlar fabric. (a) 3D image, and (b) profile along the printing direction (the x-axis).

# 3.2 Printability of PEDOT:PSS-PEO on Kevlar textile by means of eDIW.

The experimental results revealed that when the standoff distance H was smaller than the inner diameter of the needle [50 µm, Fig. 5(a)], it was possible to print PEDOT:PSS-PEO on Kevlar textile at low printing speeds ( $U < 100 \, \text{mm/s}$ ) without an external electric field ( $V = 0 \, \text{kV}$ ). However, as the printing speed increased, the printed lines broke up during the printing. When the value of H was twice the needle inner diameter [Fig. 5(b)], no intact lines could be printed by DIW, without applying an external electric field. Nevertheless, after the value of H was increased further[(to four times the inner diameter, Fig. 5(c)], the material could be printed on the substrate at lower printing speeds ( $U < 50 \, \text{mm/s}$ ) than those in the case of  $H = 30 \, \text{µm}$ .

With an external electric field applied (V > 0 kV), the printability was significantly enhanced as is attested by Fig. 4. When  $H = 30 \text{ }\mu\text{m}$  [Fig. 5(a)], the range of printable speed increased from 100 to 400 mm/s at V = 4.42 kV at the governing electrode. However, the effectiveness of the electric field diminished as the value of H increased. When  $H = 100 \text{ }\mu\text{m}$  [Fig. 5(b)], an increase in the voltage V expanded the printable U range from [non-printable] to [0–300 mm/s] at 3.76 kV. However, the printable U range was narrowed down to 0–200 mm/s at a higher voltage applied (4.55 kV). When  $H = 200 \text{ }\mu\text{m}$  [Fig. 5(c)], the electric field could increase the maximum printable speed from 50 to 200 mm/s. Although there are differences in the effectiveness of a high voltage applied, it is evident that the external electric field facilitated and broadened the printable ranges in eDIW.





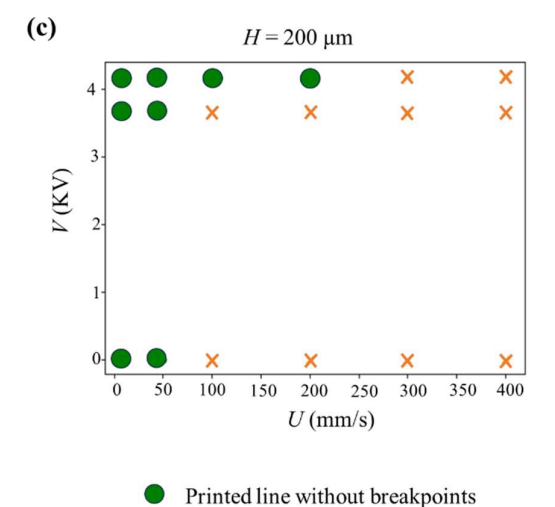


Fig. 5. Printability of PEDOT:PSS-PEO via eDIW versus the applied voltage V, printing speed U with the standoff distance H of (a) 30  $\mu$ m, (b) 100  $\mu$ m, and (c) 200  $\mu$ m.

Printed line with breakpoints

As is illustrated in Fig. 5, when V < 3 kV, the printing process failed with line break-up failures, or the printed lines with a very large width. Accordingly, to analyze the relationship between the line width and the corresponding resistivity of the printed lines, 23 cases at V = 0 kV or at V > 3 kV were explored. The parameter settings for eDIW of the selected cases are listed in Table 1. For each case, three

different replicates were performed and the deviations in the width values W were recorded.

Table 1: Parameter settings for eDIW in the selected cases (V = 0 kV or V > 3 kV) and the widths W of the printed lines. U is the printing speed, H is the stand-off distance,  $L_1$  is the horizontal distance between the electrode and the needle,  $L_2$  is the vertical distance between the electrode and the end of the needle, and V is the voltage applied.

needle, and v is the voltage applied.						
Experiment	Process parameter setting					$W(\mu m)$
#	U	Н	$L_{I}$	$L_2$	V	
	(mm/s)	(µm)	(mm)	(mm)	(kV)	
1	10	30	1.59	1.02	0	385.3±27.8
2	50	30	1.59	1.02	0	194.1±26.6
3	100	30	1.59	1.02	0	107.3±12.8
4	200	30	1.59	1.02	3.21	28.9±4.73
5	200	30	1.59	1.02	4.42	33.9±8.3
6	300	30	1.59	1.02	4.42	19.9±4.91
7	400	30	1.59	1.02	4.42	19.7±3.36
8	10	100	1.65	1.11	3.76	153.5±23.1
9	50	100	1.65	1.11	3.76	61.7±14.7
10	100	100	1.65	1.11	3.76	47.5±1.41
11	200	100	1.65	1.11	3.76	31.7±8.75
12	300	100	1.65	1.11	3.76	20.8±4.37
13	10	100	1.65	1.11	4.55	119.3±18.1
14	50	100	1.65	1.11	4.55	62.5±9.4
15	200	100	1.65	1.11	4.55	25.5±6.33
16	10	200	1.55	1.20	0	158.1±28.7
17	50	200	1.55	1.20	0	77.4±12.6
18	10	200	1.55	1.20	3.67	138.2±20.2
19	50	200	1.55	1.20	3.67	58.1±18.1
20	10	200	1.55	1.20	4.2	156.2±20.7
21	50	200	1.55	1.20	4.2	51.6±14.1
22	100	200	1.55	1.20	4.2	42.9±12.5
23	200	200	1.55	1.20	4.2	31.6±8.46

# 3.3 Widths of printed PEDOT: PSS-PEO lines under different eDIW process settings

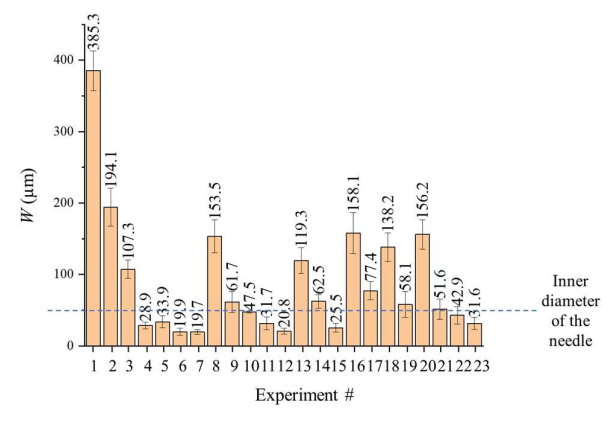


Fig. 6. Widths W of the printed PEDOT:PSS-PEO lines drawn by eDIW. The eDIW printing process settings in each particular experiment # are listed in

The external electric field not only expanded the printable windows of the process parameters in eDIW but also allowed printing of thinner and narrower conductive lines with a higher resolution in both the line width and height. Figure 6 presents the widths W of the printed lines in each case. In the absence of the electrical field (# = 1, 2, 3, 16, 17), essentially, as in the conventional DIW method, the widths W of the printed lines on

Kevlar was larger than the needle's inner diameter ( $\sim 50~\mu m$ ). It was attributed to viscoelasticity of the PEDOT:PSS-PEO ink, resulting in a significant die swell caused by elastic forces. The literature suggests that by careful tuning of the printing speed and the stand-off distance, it might be possible to achieve a narrower line with a width smaller than the extrusion orifice diameter, e.g., 60% of the needle inner diameter [32]. However, the inherently rough surface of the Kevlar fabric posed greater challenges for achieving narrow lines compared to the previous study which used a smooth substrate. Accordingly, merely adjusting H and U in DIW process did not facilitate formation of precise line widths on a rough substrate.

By applying an electric field during the printing process (i.e., using eDIW), remarkable improvements in the printed line width were observed in this study. As illustrated in Fig. 6, when  $H=30~\mu m$  (#=4–7), the smallest line width that could be printed was  $W=19.7~\mu m$  at U=400~mm/s, which is 39.4% of the inner diameter of the needle. When  $H=100~\mu m$  (#=8–15), the smallest value of W was 25.5  $\mu m$  at U=300~mm/s, which is 51% of the inner diameter of the needle. When  $H=200~\mu m$  (#=18–23), the smallest value of W was 31.6  $\mu m$ , which is about 63.2 % of the inner diameter of the needle at U=200~mm/s.

To further investigate the dependence of the printed line width W on the printing speed U, the entire set of experimental data was segregated into seven groups, each distinguished by different process parameters including H,  $L_1$ ,  $L_2$ , and V, as detailed in Table 2.

Table 2. Several groups distinguished by different process parameters for eDIW including stand-off distance H, horizontal  $L_1$  and vertical  $L_2$  distances between the electrode and the needle, respectively, and the voltage applied V.

		, <sub>F</sub>	,,	gFF
Group	H(µm)	$L_l(mm)$	$L_2(mm)$	V(kV)
number				
Group 1	30	1.59	1.02	0
Group 2	30	1.59	1.02	4.42
Group 3	100	1.65	1.11	3.76
Group 4	100	1.65	1.11	4.55
Group 5	200	1.55	1.20	0
Group 6	200	1.55	1.20	3.67
Group 7	200	1.55	1.20	4.20

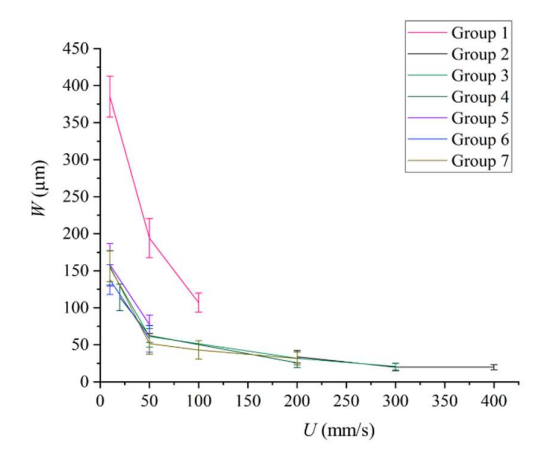


Fig. 7. Width W of the PEDOT:PSS-PEO lines decreases with the increase of the eDIW printing speed U. The eDIW experiment settings for each group are listed in Table 2.

Figure 7 presents a consistent trend in the width W of the printed PEDOT:PSS-PEO lines for all experimental conditions with varying printing speeds U. In all cases, W decreased approximately exponentially as U increased. It was observed that the value of H significantly affected the results when the value of U was below 100 mm/s. For instance, when the value of H was 30  $\mu$ m (60% of the inner diameter of the needle), the value of W was nearly doubled compared to the one corresponding to  $H = 100 \mu m$  (200% of the inner diameter), or to  $H = 200 \mu m$  (400% of the inner diameter), even at the same U. However, when the value of H was set at 100  $\mu$ m and 200  $\mu$ m (Groups 3–7), the value of W remained the same at the same U. For example,  $W = 153.5 \mu \text{m}$  when U = 10 mm/s and H = 10 mm/s100  $\mu$ m and  $W = 158.1 \ \mu$ m when  $U = 10 \ \text{mm/s}$  and  $H = 200 \ \text{mm/s}$ μm. When U surpassed 200 mm/s, W decreased to the level of the inner diameter of the needle. At this point, the value of Hwas immaterial in respect to W. Indeed, with  $H = 100 \mu m$  and U = 50 mm/s, the width W = 62.5 µm, and with H = 200 µm and U = 50 mm/s, the width  $W = 51.6 \mu m$ . Furthermore, with the printing speed below 300 mm/s, the width W remained nearly constant when U = 300, and 400 mm/s, indicating a lower threshold for W on this substrate.

Figure 8 presents a series of microscope images of printed lines with various widths on Kevlar fabric. It is seen that as the line width decreased, the effect of the substrate on both the side edge and line surface (in top view) became more pronounced.

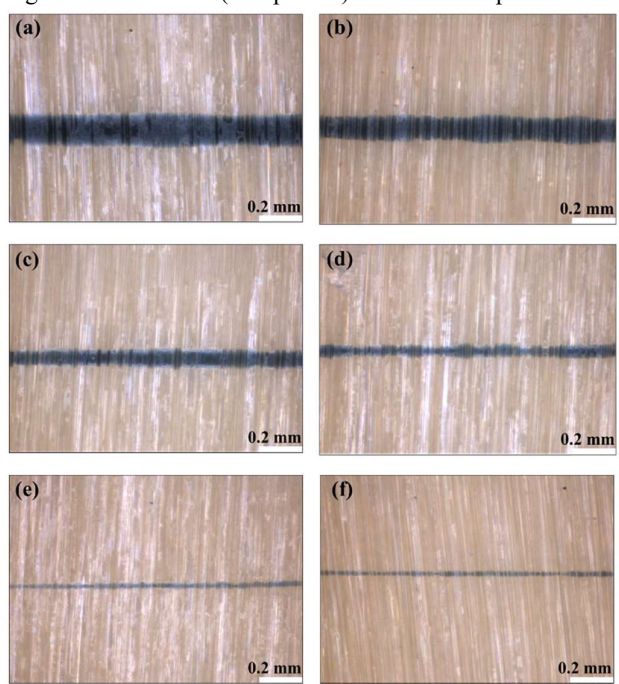


Fig. 8. Optical microscope images of PEDOT:PSS-PEO lines on Kevlar at different eDIW printing parameters, such as the printing speed U, the stand-off distance H, and the applied voltage V. The corresponding parameters are listed in Table 1 with their measured width W. Panel (a) case 20, (b) case 13, (c) case 17, (d) case 19, (e) case 15, and (f) case 7.

3.4 ANOVA analysis of the effects of the stand-off distance, the printing speed, and the electric field strength on the printed line width

Table 3 displays the results of the ANOVA analysis of the effects of the stand-off distance H, the printing speed U, and

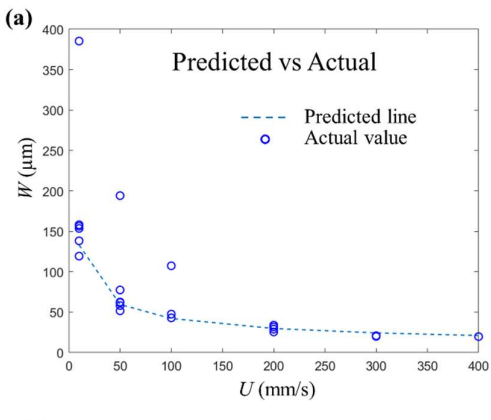
the applied voltage V on the printed line width. A 95% confidence interval was adopted in this analysis. From Table 3 it follows that only U has a P value smaller than 0.05, indicating a significant influence on the line width. The effects of H and V are not as significant, which agrees with the plots presented in Fig. 7.

Table 3. ANOVA for means-printed line width according to such parameters as the stand-off distance *H*, the printing speed *U*, and the applied voltage *V*.

		, F	, _ F ,		
Factor	DoF	Adj SS	Adj MS	F	P
Н	2	8636	4316	0.59	0.564
U	6	93627	15605	4.07	0.012
V	6	67885	11314	2.08	0.114
,	Ü	0,000	11011	2.00	٠.

## 3.5 Comparison of predicted and experimental results.

Fig. 9(a) shows that the predicted values closely match the actual values, except when the H is significantly less than the needle's inner diameter at low speeds. RMSD of the predicted line is 0.386, which is considered acceptable. Additionally, the residuals are randomly distributed without discernible patterns, confirming that the printing speed is an independent parameter influencing the width of the printed lines. The predictive model serves as a valuable tool for future work, aiding in the design of experimental settings to achieve the desired line width. It also provides critical evidence that increasing the DIW printing speed is key to attaining higher resolution in printed lines, surpassing the limitations imposed by the needle gauge.



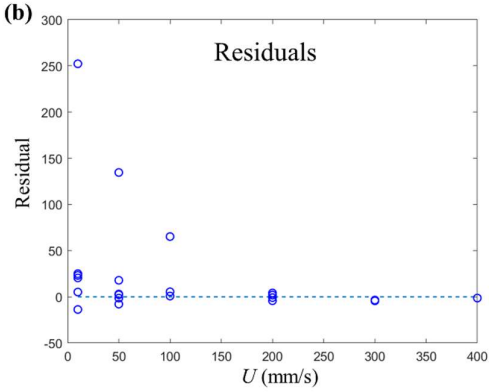


Fig. 9. (a) Comparison of predicted and actual values. (b) Residual analysis plot.

#### 3.6 Resistivity of the printed PEDOT:PSS-PEO lines

To characterize the effect of the additional polymer (i.e., PEO) on the resistivity  $\rho$  of the printed lines, pure PEDOT:PSS, was prepared and characterized for the sake of comparison. Additionally, the experiments were conducted by using four different sizes of needles: 22 gauge (i.e., 413 µm inner diameter), 23 gauge (337 µm), 26 gauge (260 µm), and 34 gauge (50 µm) to implement and investigate a wide range of line widths, in the 20 to 1400 µm range. It was observed that for pure PEDOT:PSS,  $\rho$  remained relatively constant, at around  $1.5 \times 10^{-2} \Omega$  m when the cross-sectional area exceeded  $3.4 \times 10^{3}$ μm² (Fig. 10). However, as the cross-sectional area decreased, the resistivity abruptly increased, likely due to an increase in the contact resistance. In contrast, the average resistivity of lines printed with the PEDOT:PSS-PEO ink was approximately  $2.49\times10^{-3}$   $\Omega$  m (Fig. 11), which is only about 16.6% of the resistivity of lines printed using pure PEDOT:PSS consistent with our previous work [22]. However, even though the same ink formulation was used, there is a significant difference in the resistivity value of printed lines measured in this study and the previous study [22]. The average resistivity of the printed lines in our previous study was about  $7 \times 10^{-4} \Omega$  m, much smaller than the value of  $2.49 \times 10^{-3}$   $\Omega$  m measured in this work. The observed difference can be attributed to the change in substrate from a glass slide, as used in our previous work, to a Kevlar fabric in this study. The Kevlar fabric is considerably rougher and more porous, leading to increased contact resistance. Furthermore, on Kevlar, the line undulates over fibers, making it effectively longer than it appears in a top view (Fig. 12). This results in a higher overall measured resistivity.

Table 4. Resistivity  $\rho$  (the average value with a standard deviation) for printed PEDOT:PSS lines with different width W and cross-sectional area A.

W(µm)	$A (\times 10^4 \mu m^2)$	$\rho  (m\Omega  m)$
1400.8	4.1	$15 \pm 0.7$
1298.1	2.4	$16 \pm 2.9$
702.6	0.93	$19 \pm 1.1$
284.2	0.34	$45 \pm 4.3$

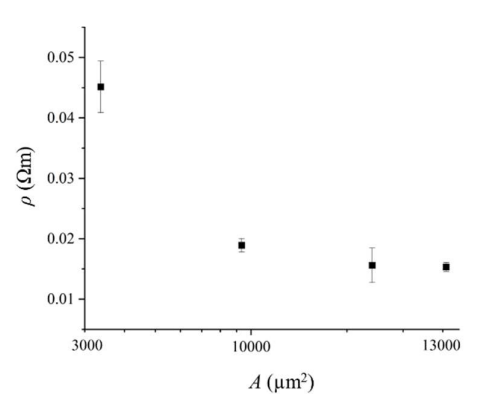


Fig. 10. PEDOT:PSS's resistivity ( $\rho$ ) vs. area (A).

Table 5. Resistivity  $\rho$  (the average with a standard deviation) of the printed PEDOT:PSS-PEO lines of different width W and cross-sectional area A.

$W(\mu m)$	$A (\times 10^4  \mu m^2)$	$\rho  (m\Omega  m)$
634.1	1.3	$2.5 \pm 0.6$
313.3	1.1	$2.2 \pm 0.3$
205.2	96	$2.9 \pm 0.2$
147.2	33	$1.3 \pm 0.8$
90.9	220	$3.3 \pm 1.2$

77.4	3400	$3.1 \pm 0.2$
19.7	27000	$1.9 \pm 0.1$

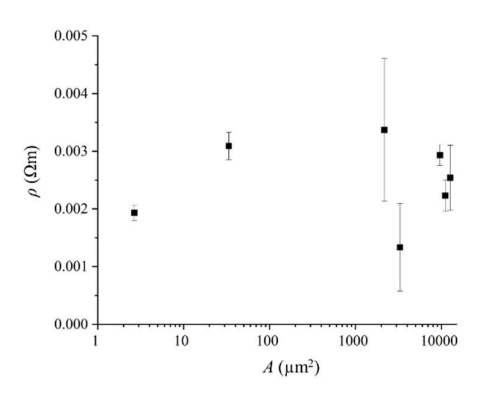


Fig. 11. Resistivity  $\rho$  vs. the cross-sectional area A of PEDOT:PSS-PEO lines drawn by eDIW.

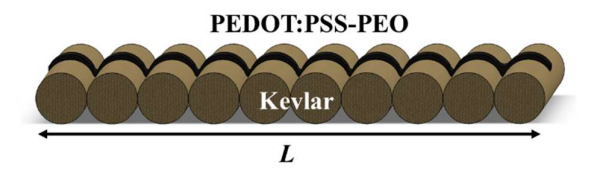


Fig. 12. Schematics of the printed lines on Kevlar fabric.

In Fig. 13, an LED circuit was employed to ascertain the electrical conductivity of printed PEDOT:PSS-PEO lines, and its potential for wearable electronics. One end of LED was connected directly to an end of the line and the other ends were connected to a power supply. The LED light was OFF with 0 V as in Fig. 13(a), and ON at 4.0 V, when the LED was lit up, as in Fig. 13(b).





Fig. 13. (a) LED light is OFF when the power supply is off. (b) LED light is ON when the power supply is ON with 4.0V applied.

#### 4. Conclusion

In this study, we studied in detail the electric field-assisted direct ink writing (eDIW) process developed in our previous work. An electrically conductive PEDOT:PSS-PEO mixture was deposited on Kevlar fabric, with a high resolution (e.g., 20 µm line width) and high robustness even at 400 mm/s printing speed. By the conventional DIW process (without external electric field applied), intact lines on Kevlar could not be printed successfully except when the stand-off distance was less than the inner diameter, and only at a low printing speed (e.g., < 100 mm/s). On the other hand, in eDIW where an external electric field was applied during the printing process, intact lines could always be printed on Kevlar fabric substrate

under a wide range of printing conditions, such as high printing speeds and long stand-off distances.

Three pivotal factors (the stand-off distance, the electric field strength, and the printing speed) were identified that govern the width of the printed lines during the eDIW process. Notably, an external electric field increased the working range of the printing speed and simultaneously eliminated the dieswell effect when printing viscoelastic inks issued from small needles. Accordingly, line widths smaller than the needle orifice were successfully printed facilitated by an external electric force.

Not only the width of the printed lines, but also the substrate where the lines were deposited affected the resistivity of the lines drawn. There was a higher resistivity between lines drawn on a Kevlar fabric and those drawn on Kapton film, possibly because of the rough Kevlar fabric substrate, also because the rough and porous substrate caused the lines to be longer than those on Kapton film. Still, the resistivity of the lines of PEDOT:PSS-PEO ink on Kevlar fabric was sufficiently low, i.e.,  $\sim 2.49 \times 10^{-3} \Omega$  m, to light LED.

This study reveals great promise of conducting PEDOT:PSS-PEO inks in the framework of the eDIW technique for micro-scale electronic fabrication on textiles. In future work, we plan to apply the optimal printing parameters identified in this study to produce complex, customized designs for multifunctional sensors on textiles.

#### Acknowledgements

This project was supported by National Science Foundation (NSF) Grant 2224749.

#### References

- [1] Hughes-Riley, T., Dias, T., & Cork, C. (2018). A historical review of the development of electronic textiles. Fibers, 6(2), 34.
- [2] Dong, J., Tang, X., Peng, Y., Fan, C., Li, L., Zhang, C., Lai, F., He, G., Ma, P., Wang, Z., Wei, Q., Yan, X., Qian, H., Huang, Y., & Liu, T. (2023). Highly permeable and ultrastretchable E-textiles with EGaIn-superlyophilicity for on-skin health monitoring, joule heating, and electromagnetic shielding. Nano Energy, 108, 108194.
- [3] Karamuk, E., Mayer, J., Düring, M., Wagner, B., Bischoff, B., Ferrario, R., Billia, M., Seidl, R., Panizzon, R., & Wintermantel, E. (2001). Embroidery technology for medical textiles. In Medical Textiles (pp. 200-206). Woodhead Publishing, UK.
- [4] Winterhalter, C. A., Teverovsky, J., Wilson, P., Slade, J., Horowitz, W., Tierney, E., & Sharma, V. (2005). Development of electronic textiles to support networks, communications, and medical applications in future US Military protective clothing systems. IEEE Transactions on Information Technology in Biomedicine, 9(3), 402-406
- [5] Krueger, G. P., & Banderet, L. E. (1997). Effects of chemical protective clothing on military performance: a review of the issues. Military Psychology, 9(4), 255-286.
- [6] Torvi, D. A., & Hadjisophocleus, G. V. (1999). Research in protective clothing for firefighters: state of the art and future directions. Fire Technology, 35, 111-130.
- [7] Raheel, M. (Ed.). (1994). Protective Clothing Systems and Materials (Vol. 25). CRC Press, USA.
- [8] Pani, D., Achilli, A., & Bonfiglio, A. (2018). Survey on textile electrode technologies for electrocardiographic (ECG) monitoring, from metal wires to polymers. Advanced Materials Technologies, 3(10), 1800008.
- [9] Afroj, S., Tan, S., Abdelkader, A. M., Novoselov, K. S., & Karim, N. (2020). Highly conductive, scalable, and machine washable graphene-based E-textiles for multifunctional wearable electronic applications. Advanced Functional Materials, 30(23), 2000293.
- [10] Kim, H. K., Kim, M. S., Chun, S. Y., Park, Y. H., Jeon, B. S., Lee, J. Y., Hong, Y.K., Joo, J., & Kim, S. H. (2003). Characteristics of

- electrically conducting polymer-coated textiles. Molecular Crystals and Liquid Crystals, 405(1), 161-169.
- [11] Tran, V. V., Lee, S., Lee, D., & Le, T. H. (2022). Recent developments and implementations of conductive polymer-based flexible devices in sensing applications. Polymers, 14(18), 3730.
- [12] Xu, S., Shi, X. L., Dargusch, M., Di, C., Zou, J., & Chen, Z. G. (2021). Conducting polymer-based flexible thermoelectric materials and devices: From mechanisms to applications. Progress in Materials Science, 121, 100840.
- [13] Xu, S., Shi, X. L., Dargusch, M., Di, C., Zou, J., & Chen, Z. G. (2021). Conducting polymer-based flexible thermoelectric materials and devices: From mechanisms to applications. Progress in Materials Science, 121, 100840.
- [14] Dominguez-Alfaro, A., Gabirondo, E., Alegret, N., De León-Almazán, C. M., Hernandez, R., Vallejo-Illarramendi, A., Prato, M., & Mecerreyes, D. (2021). 3D printable conducting and biocompatible PEDOT-graft-PLA copolymers by direct ink writing. Macromolecular Rapid Communications, 42(12), 2100100.
- [15] Dong, Q., Zhou, Y., Pei, J., Liu, Z., Li, Y., Yao, S., Zhang, J., & Tian, W. (2010). All-spin-coating vacuum-free processed semi-transparent inverted polymer solar cells with PEDOT: PSS anode and PAH-D interfacial layer. Organic Electronics, 11(7), 1327-1331.
- [16] Hwang, B., Lund, A., Tian, Y., Darabi, S., & Muller, C. (2020). Machine-washable conductive silk yarns with a composite coating of Ag nanowires and PEDOT: PSS. ACS Applied Materials & Interfaces, 12(24), 27537-27544...
- [17] Oh, J. Y., Shin, M., Lee, J. B., Ahn, J. H., Baik, H. K., & Jeong, U. (2014). Effect of PEDOT nanofibril networks on the conductivity, flexibility, and coatability of PEDOT: PSS films. ACS applied materials & interfaces, 6(9), 6954-6961.
- [18] Oh, S. H., Heo, S. J., Yang, J. S., & Kim, H. J. (2013). Effects of ZnO nanoparticles on P3HT: PCBM organic solar cells with DMF-modulated PEDOT: PSS buffer layers. ACS applied materials & interfaces, 5(22), 11530-11534..
- [19] Sanviti, M., Mester, L., Hillenbrand, R., Alegria, A., & Martínez-Tong, D. E. (2022). Solvent-structured PEDOT: PSS surfaces: Fabrication strategies and nanoscale properties. Polymer, 246, 124723.
- [20] Yildirim, E., Wu, G., Yong, X., Tan, T. L., Zhu, Q., Xu, J., Ouyang, J., Wang, J.S., & Yang, S. W. (2018). A theoretical mechanistic study on electrical conductivity enhancement of DMSO treated PEDOT: PSS. Journal of Materials Chemistry C, 6(19), 5122-5131.
- [21] Wang, X., Plog, J., Lichade, K. M., Yarin, A. L., & Pan, Y. (2023). Three-dimensional printing of highly conducting PEDOT: PSS-based

- polymers. Journal of Manufacturing Science and Engineering, 145(1), 011008
- [22] Plog, J., Wang, X., Lichade, K. M., Pan, Y., & Yarin, A.L. (2023). Extremely-Fast Electrostatically-Assisted Direct Ink Writing of 2d, 2.5 d and 3d Functional Traces of Conducting Polymer Poly (3, 4-Ethylenedioxythiophene) Polystyrene Sulfonate-Polyethylene Oxide (Pedot: Pss-Peo). Available at SSRN 4308026.
- [23] Balagna, C., Irfan, M., Perero, S., Miola, M., Maina, G., Santella, D., & Simone, A. (2017). Characterization of antibacterial silver nanocluster/silica composite coating on high performance Kevlar® textile. Surface and Coatings Technology, 321, 438-447.
- [24] Maithani, Y., Mehta, B. R., & Singh, J. P. (2023). PEDOT: PSS-treated laser-induced graphene-based smart textile dry electrodes for longterm ECG monitoring. New Journal of Chemistry, 47(4), 1832-1841.
- [25] Choi, C. M., Kwon, S. N., & Na, S. I. (2017). Conductive PEDOT: PSS-coated poly-paraphenylene terephthalamide thread for highly durable electronic textiles. Journal of Industrial and Engineering Chemistry, 50, 155-161.
- [26] Tao, X., Koncar, V., & Dufour, C. (2011). Geometry pattern for the wire organic electrochemical textile transistor. Journal of the Electrochemical Society, 158(5), H572.
- [27] Saadi, M. A. S. R., Maguire, A., Pottackal, N. T., Thakur, M. S. H., Ikram, M. M., Hart, A. J., Ajayan, P.M., & Rahman, M. M. (2022). Direct ink writing: a 3D printing technology for diverse materials. Advanced Materials, 34(28), 2108855.
- [28] Yuk, H., Lu, B., Lin, S., Qu, K., Xu, J., Luo, J., & Zhao, X. (2020). 3D printing of conducting polymers. Nature Communications, 11(1), 1604
- [29] Wu, K., Kim, K. W., Kwon, J. H., Kim, J. K., Kim, S. H., & Moon, H. C. (2023). Direct ink writing of PEDOT: PSS inks for flexible microsupercapacitors. Journal of Industrial and Engineering Chemistry, 123, 272-277.
- [30] Plog, J., Jiang, Y., Pan, Y., & Yarin, A. L. (2021). Electrostatically-assisted direct ink writing for additive manufacturing. Additive Manufacturing, 39, 101644.
- [31] Plog, J., Wang, X., Pan, Y., & Yarin, A. L. (2022). Electrostatically-assisted direct ink writing with superior speed and resolution. Journal of Manufacturing Processes, 76, 752-757.
- [32] Yuk, H., & Zhao, X. (2018). A new 3D printing strategy by harnessing deformation, instability, and fracture of viscoelastic inks. Advanced Materials, 30(6), 1704028.